Chemical Science

ROYAL SOCIETY OF CHEMISTRY

EDGE ARTICLE

View Article Online
View Journal | View Issue

Cite this: *Chem. Sci.*, 2021, **12**, 8512

All publication charges for this article have been paid for by the Royal Society of Chemistry

Triarylamine-based porous coordination polymers performing both hydrogen atom transfer and photoredox catalysis for regioselective α-amino C(sp^3)–H arylation†

Hanning Li, Yang Yang, Xu Jing, * Cheng He and Chunying Duan *

Direct functionalization of C(sp^3)–H bonds in a predictable, selective and recyclable manner has become a central challenge in modern organic chemistry. Through incorporating different triarylamine-containing ligands into one coordination polymer, we present herein a heterogeneous approach to the combination of hydrogen atom transfer (HAT) and photoredox catalysis for regioselective C–H arylation of benzylamines. The different molecular sizes and coordination modes of the ligands, tricarboxytriphenylamine (H_3**TCA**) and tris(4-(pyridinyl)phenyl)amine (**NPy$_3$**), in one coordination polymer consolidate the triarylamine (Ar_3N) moiety into a special structural intermediate, which enhances the chemical and thermal stability of the polymers and diminishes structural relaxation during the catalytic process. The inherent redox potentials of Ar_3N moieties prohibit the *in situ* formed $Ar_3N^{\bullet+}$ to earn an electron from C(sp^3)–H nucleophiles, but allow the abstraction of a hydrogen atom from C(sp^3)–H nucleophiles, enabling the formation of the C(sp^3)$^\bullet$ radical and the cross-coupling reaction to proceed at the most electron-rich sites with excellent regioselectivity. The new heterogeneous photoredox HAT approach skips several interactions between transient species during the typical synergistic SET/HAT cycles, demonstrating a promising redox-economical and reagent-economical heterogeneous platform that has not been reported for α-amino C–H arylation to form benzylamine derivatives. Control experiments based on monoligand coordination polymers suggested that the mixed-ligand approach improved the photochemical and photophysical properties, providing important insight into rational design and optimization of recyclable photocatalysts for rapid access to complex bioactive molecules and late-stage functionalized pharmaceuticals.

Received 10th February 2021
Accepted 11th May 2021

DOI: 10.1039/d1sc00828e

rsc.li/chemical-science

Introduction

The use of C(sp^3)–H bonds, which are ubiquitous in organic molecules, as latent nucleophile equivalents for cross-coupling reactions has the potential to substantially streamline synthetic efforts in organic chemistry.[1,2] Visible-light photocatalysis has led to a paradigm shift in organic synthesis that encompasses the activation of small molecules,[3–7] fostering the discovery of promising tools to activate aliphatic C–H bonds; however, functionalization of C(sp^3)–H bonds in a predictable, selective, and efficient manner remains a central challenge.[8,9] Hydrogen atom transfer (HAT),[10–12] when involved in photocatalysis, can activate organic substrates without the limitation of redox potentials, allowing kinetically controlled functionalization of hydridic C–H bonds in the presence of other weaker, polarity-mismatched ones. However, besides the limits of photocatalysts capable of performing single electron transfer and hydrogen atom transfer (SET/HAT) synergistic catalysis in a homogeneous fashion,[13,14] developing efficient heterogeneous photocatalytic systems[15,16] to expand the real applications in organic syntheses and the fine chemicals industry remains largely unexplored, partly due to the difficulties in controlling the kinetics of the multistep electron transfer or hydrogen atom transfer catalytic cycles in a heterogeneous fashion.[17]

Porous coordination polymers with ordered photoactive organic ligands and inorganic nodes are well-known for their promising catalytic performance.[18–22] The regular distribution of photocatalytic sites in confined environments benefits the fixation and stabilization of the active radicals formed under light-irradiation to overcome the restrictions in a homogeneous system.[23–25] Taking advantage of Ar_3N-based coordination polymers for photocatalysis with excellent photocatalytic performance and recyclability[26–28] and the tertiary amine radical cation (*i.e.*, quinuclidine radical) capable of engendering

State Key Laboratory of Fine Chemicals, Zhang Dayu College of Chemistry, Dalian University of Technology, 116024, P. R. China. E-mail: xjing@dlut.edu.cn; cyduan@dlut.edu.cn

† Electronic supplementary information (ESI) available. CCDC 1970513, 1970515, 1970516 and 1970538. For ESI and crystallographic data in CIF or other electronic format see DOI: 10.1039/d1sc00828e

a selective HAT at the most electron-rich site of C(sp^3)–H nucleophiles,[29] we envisioned that incorporating triarylamine (Ar_3N) moieties into one coordination polymer would combine HAT and photoredox catalysis for regioselective C(sp^3)–H functionalization at electron-rich C–H sites.

It is noted that organic dyes with Ar_3N have never been used as HAT catalysts in a homogeneous fashion, partly due to the heavy structural relaxation[30] from $Ar_3N^{\bullet+}$ to Ar_3NH^+ limiting the kinetics of H-atom exchange in solution. To avoid the potential structural relaxation during the HAT process, tertiary amine HAT catalysts, such as quinuclidine,[29,31,32] were always constrained in a robust sp^3 conformation. Alternatively, the efficiency of the photocatalytic conversions using Ar_3N-based chromophores is dependent on the planar conformation of the N-center in Ar_3N chromophores essentially. Our approach thus focused on the modification of the N-center conformation in the Ar_3N-based coordination polymers to balance the efficiency of photosensitization with that of HAT catalysis. We envisioned that incorporating both tricarboxytriphenylamine (H_3**TCA**)[33] and tris(4-(pyridinyl)phenyl)amine (**NPy$_3$**)[34] into one coordination polymer would provide the possibility of optimizing the conformation of Ar_3N moieties into a special intermediate structure that mixed the characteristics of both N(sp^3) and N(sp^2), decreasing the potential structural relaxation during the HAT process. Meanwhile, electron-rich C–H bonds adjacent to amine functionalities could serve as useful precursors to form the C-centered radical C(sp^3)$^\bullet$ *via* a HAT event when interacting with the aforementioned catalytically generated amine radical cation.[35,36]

The proposed catalytic strategy was evaluated by the activation of an *N*-benzylic C(sp^3)–H bond, as benzylic amines are important pharmaceutical structural motifs that are difficult to access *via* simple substrates. The mechanistic details are outlined in Fig. 1. Irradiation of polymers containing Ar_3N moieties produces a strongly reductive Ar_3N^* ($E_{red} = -2.04$ V, *vs.* Ag/AgCl) that initially undergoes SET with an electron-deficient radical precursor, 1,4-dicyanobenzene (1,4-DCB, $E^{red}_{1/2} = -1.61$ V, *vs.* SCE),[37] to afford the corresponding anionic radical (sub1$^{\bullet-}$) and the oxidized photosensitizer $Ar_3N^{\bullet+}$. The latter selectively abstracts a H atom from the substrate that contains a C(sp^3)–H bond with a lower C–H bond dissociation energy (BDE) to form C(sp^3)$^\bullet$, as the inherent moderate oxidization potential of $Ar_3N^{\bullet+}$ prohibits the direct oxidation of substrates *via* SET. The direct coupling of the two generated organic radicals predominates the desired product at the most electron-rich site of the C–H nucleophile and completes the SET/HAT catalytic cycles. This redox-economical heterogeneous platform skipped several interactions between transient species during the reactions, allowing rapid access to complex bioactive molecules and late-stage functionalized pharmaceuticals in a recyclable manner.

Results and discussion

The solvothermal reaction of tricarboxytriphenylamine (H_3**TCA**, 0.05 mmol) and tris(4-(pyridinyl)phenyl)amine (**NPy$_3$**, 0.05 mmol) with $Cd(NO_3)_2 \cdot 4H_2O$ (0.25 mmol) gave crystals of Cd-**MIX** in a yield of approximately 50%. ^{1}H NMR of Cd-**MIX** in

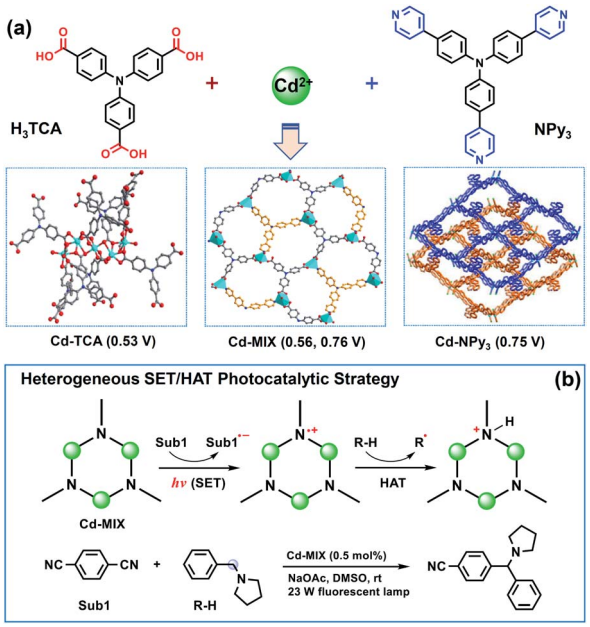

Fig. 1 (a) The mixed-ligand strategy for the construction of coordination polymers showing the structures of the two ligands mentioned and the measured oxidative potentials (*vs.* Ag/AgCl) (in parentheses) of the coordination polymers. (b) Schematic illustration of the heterogeneous SET/HAT photocatalytic approach in which the *in situ* formed oxidized $Ar_3N^{\bullet+}$ in mixed-ligand Cd-**MIX** acts as a HAT catalyst for regioselective C(sp^3)–H arylation.

DMSO-d_6/DCl gave a 2 : 1 molar ratio of **TCA**$^{3-}$ and **NPy$_3$** ligands in the structure (Fig. S16†). The similar powder X-ray diffraction (PXRD) patterns based on the single-crystal and as-synthesized Cd-**MIX** indicated that the bulk Cd-**MIX** consisted of a pure phase (Fig. S17†). Changing the molar ratio of the two ligands does not affect the structure of Cd-**MIX**, but affects its purity and yield. Single-crystal analysis revealed that Cd-**MIX** crystallized in the *C*2/*c* space group, and the asymmetric unit of Cd-**MIX** comprised three independent Cd ions, one **NPy$_3$**, and two **TCA**$^{3-}$ ligands. Both Cd1 and Cd3 were six-coordinated by one N atom from **NPy$_3$**, four O atoms from carboxylates, and one O atom from H_2O molecules (Fig. 2a). However, Cd2 was seven-coordinated by one N atom from **NPy$_3$**, four O atoms from two bidentate carboxylates, and two O atoms from bridged carboxylates. The carboxylates connected Cd1 and Cd2 together to form tetranuclear clusters. The propeller-like **TCA**$^{3-}$ ligands coordinated to the clusters and Cd3 to generate a 3D coordination polymer with channel openings of 8.6 × 13.0 Å^2 (Fig. 2c). The **NPy$_3$** ligand coordinated with three different Cd ions and was positioned in a conformation consolidated by the **TCA**$^{3-}$-linked Cd nodes (Fig. 2b). Obvious π···π stacking interactions between the two ligands were also found to stabilize the mixed-ligand coordination polymer with the interplanar separation reaching 3.62 Å (Fig. S4†).

Detailed structural analysis revealed that the included angles around the central nitrogen atom N2 of the **NPy$_3$** ligands in Cd-**MIX** were 121.3, 123.4, and 115.0°. The structural constraints consolidated the central N2 atom which was positioned 0.36 Å

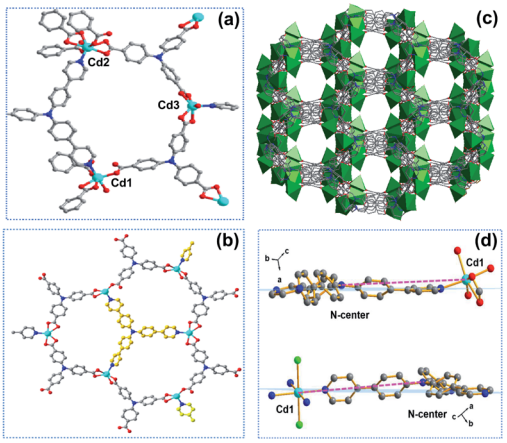

Fig. 2 (a) Coordination environments of Cd ions with related TCA^{3-} and NPy_3 ligands in Cd-**MIX**. (b) The structural constraints of NPy_3 ligands consolidated by the coordination of TCA^{3-} with Cd ions in Cd-**MIX**. (c) Structure of Cd-**MIX** showing the 3D framework with channel openings of 8.6 × 13.0 $Å^2$. (d) The conformations of the NPy_3 ligand in Cd-**MIX** (top) and Cd-NPy_3 (bottom). Hydrogen atoms and solvent molecules are omitted for clarity. Cyan, Cd; red, O; blue, N; gray, C; green, Cl.

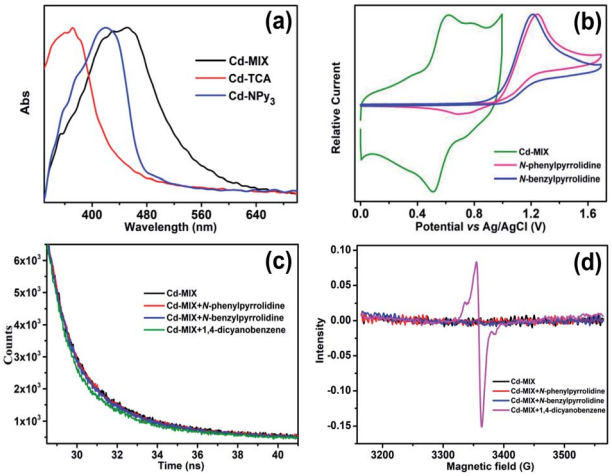

Fig. 3 (a) Solid-state UV-vis spectra of Cd-**MIX**, Cd-**TCA**, and Cd-**NPy3**. (b) Cyclic voltammetry of Cd-**MIX** in the solid state and amines examined in solution. Fluorescence decay curves (c) and EPR spectra (d) of Cd-**MIX** suspension with and without **1a**, **1c**, and 1,4-dicyanobenzene, respectively.

above the plane defined by the other three N atoms (Fig. S10†). The conformation of NPy_3 thus was fixed as a special structural intermediate that mixed both N(sp^3) and N(sp^2) characteristics of the central N atom, which is beneficial for the transformation from $Ar_3N^{\bullet+}$ to Ar_3NH^+ to abstract a hydrogen atom at the most electron-rich site of C(sp^3)–H nucleophiles. The average distance between the central N2 atom and NPy_3 ligand-bridged Cd ions (Cd···N2 distance *ca.* 10.7 Å) in Cd-**MIX** was approximately 0.2 Å shorter than that of the monoligand coordination polymer Cd-NPy_3, which is assembled from only the NPy_3 ligand (Fig. 2d), further confirming a distorted conformation in the mixed-ligand coordination polymer.[38,39]

Moreover, the d^{10} structure of the Cd centers as well as the variable bridging mode between the two kinds of ligands and the metal nodes brought some flexible elements, allowing the inherent structural relaxation to occur in the solid state in a controllable way during the hydrogen atom transfer process. The free volume in the desolvated coordination polymer Cd-**MIX** is approximately 43.5%, as determined by PLATON.[40] Dye uptake experiments performed by soaking Cd-**MIX** crystals in a methylene blue solution exhibited 8.0% uptake based on crystal weight. The uniform distribution of methylene blue throughout the crystals suggested that these dye molecules penetrated deeply into these channels (Fig. S22 and S23†), revealing the porosity of Cd-**MIX** for guest accommodation.[41]

The solid-state ultraviolet-visible (UV-vis) absorption spectrum of Cd-**MIX** exhibited broader absorption that spanned the visible light range than those of the monoligand coordination polymers Cd-**TCA**,[42] which is assembled from ligand H_3**TCA**, and Cd-NPy_3, respectively (Fig. 3a). Similar to that in the reported mixed-ligand coordination polymers, the stacking π···π interactions between ligands and the distorting coordination geometry of the metal centers in the mixed-ligand coordination polymers resulted in an obvious redshift of the absorption band, providing the possibility of photocatalytic conversion under visible light irradiation.[43] Solid-state cyclic voltammetry revealed that Cd-**MIX** exhibited simultaneous two oxidation couples at 0.56 V and 0.76 V (*vs.* Ag/AgCl), corresponding to the oxidation of ligands TCA^{3-} and NPy_3, respectively (Fig. 3b). The inherent moderate oxidization potential of Ar_3N in the coordination polymer prohibited the oxidized state of Cd-**MIX** from earning an electron from the C(sp^3)–H nucleophiles, *i.e.*, *N*-phenylpyrrolidine (**1a**) (Fig. 3b).[44]

When excited at 420 nm, the suspension of Cd-**MIX** in acetonitrile solution exhibited a broad emission band at 508 nm (Fig. S24†). In combination with the free energy change (E^{0-0})[45,46] between the ground and excited states, which was obtained from the absorption and emission spectra of the triarylamine-based coordination polymer Cd-**MIX**, the excited state potentials were calculated to be −2.04 and −1.84 V (*vs.* Ag/AgCl) for TCA^{3-} and NPy_3 (Fig. S19†), respectively. These potentials demonstrated that the excited state of Cd-**MIX** was able to reduce the radical precursor 1,4-dicyanobenzene (−1.61 V, *vs.* SCE)[37] to form the anionic radical sub1$^{\bullet-}$ and cation radical $Ar_3N^{\bullet+}$.

1,4-Dicyanobenzene is able to quench the emission of the coordination polymer Cd-**MIX** in an acetonitrile suspension with a Stern–Volmer constant[47] of about 1.0 × 10^3 M^{-1}, demonstrating a SET from the excited state of Cd-**MIX** to the radical precursor 1,4-dicyanobenzene (Fig. S24†). No obvious emission variation could be detected when C(sp^3)–H nucleophiles *N*-phenylpyrrolidine (**1a**) and *N*-benzylpyrrolidine (**1c**) were added (Fig. S27 and S28†). Time-dependent emission decay experiments estimated a significant decrease of the emission lifetime of Cd-**MIX** from 1.40 to 1.15 ns when 1,4-dicyanobenzene was added, but no lifetime decrease could be found when *N*-phenylpyrrolidine (**1a**) and *N*-benzylpyrrolidine

(**1c**) were present (Fig. 3c). The IR spectrum of solid-state Cd-**MIX** immersed in a 1,4-dicyanobenzene solution revealed a CN stretching vibration at 2233 cm^{-1} (Fig. S29†), suggesting the direct absorption of 1,4-dicyanobenzene within the pores of Cd-**MIX**. Direct irradiation of the solid-state Cd-**MIX** adsorbed with 1,4-dicyanobenzene led to a radical signal with a *g* value of approximately 2.004 only after a minute (Fig. 3d), whereas irradiation of Cd-**MIX** itself did not cause any obvious radical signals under identical conditions in electron paramagnetic resonance experiments. We infer that the excited state of Cd-**MIX** cannot oxidize **1a** or **1c** but is able to reduce the substrate 1,4-dicyanobenzene to generate the aromatic radical for further coupling reactions.

The photocatalytic experiment was initiated with *N*-phenylpyrrolidine (**1a**) and 1,4-dicyanobenzene as starting substrates. With a 23 W household fluorescent lamp as the light source, the photocatalytic transformation of an amine gave an α-amino cyanobenzene product (**1b**) with a conversion of 90% upon 0.5 mol% (based on the Ar_3N moiety in the mixed-ligand coordination polymer) loading of Cd-**MIX** at room temperature for 12 h (Table 2). In the reaction of *N*-benzylpyrrolidine (**1c**) with 1,4-dicyanobenzene, arylation at the *N*-benzylic position gave a coupling product (**1d**) with a conversion of 93% and regioselectivity >96% under the standard reaction conditions, and almost no arylation products at the cyclic *N*-methylene position were detected (Table 1). Meanwhile, no additional activation of products **1b** and **1d** was detected, as only electron-deficient benzonitriles could be activated in this photocatalytic system.[48] In addition, no further arylation of the resulting amine products could be observed, and benzylic amine substrates were added in twice the amount to ensure the selectivity.[44] Control experiments exhibited negligible conversion in the absence of Cd-**MIX**, while no products were detected in the dark, which suggested that both the light source and Cd-**MIX** were indispensable (Tables S4 and S5,† entries 2 and 14). Cd salt, or the simple mixing of Cd salt and ligands (H_3**TCA** and **NPy$_3$**), resulted in negative activity under identical conditions (Tables S4 and S5,† entries 3–5), verifying the high photocatalytic activity of Cd-**MIX** for the C–H arylation and that the heavy structural relaxation from $Ar_3N^{\bullet+}$ to Ar_3NH^+ in a homogeneous fashion indeed limited the kinetics of H-atom exchange. With the decrease of NaOAc content, the conversion of the reaction sharply declined, whereas the replacement of NaOAc by K_2HPO_4 (with a similar pK_b in aqueous solution) hardly affected the conversion (Tables S4 and S5,† entries 12 and 13). We estimate that an appropriate weak base environment is important for neutralizing the acidic Ar_3NH^+ or HCN produced in the reaction system to obtain an efficient reaction.

Meanwhile, when triphenylamine was used as the photocatalyst with **1a** or **1c** as coupling substrates, almost no products were obtained because the free rotation of the three arms in the free triphenylamine molecules consumes the energy at the excited state and diminishes the photosensitization efficiency (Tables S4 and S5,† entries 11), in addition to the heavy structural relaxation from $Ar_3N^{\bullet+}$ to Ar_3NH^+ limiting the kinetics of H-atom exchange in solution. As the oxidative state of Ar_3N moieties in Cd-**MIX** cannot oxidize the substrates **1a** and **1c** *via* the SET process, and the BDE of Ar_3N^+–H, *i.e.*, the quinuclidine radical cation (N^+–H 100 kcal mol^{-1}),[49] is larger than that of the *N*-benzylic C–H bond (85 kcal mol^{-1}),[50] we deduced that the regioselectivity at the *N*-benzylic position was well consistent with the idea of a mechanistic switchover from SET to HAT catalysis.[44] Deuterium labelling experiments were conducted by treating *N*-((phenyl-D_5)methyl-D_2)pyrrolidine (**1c***D*) and **1c** with 1,4-dicyanobenzene in two different vessels or in one vessel under optimal conditions (Fig. 4a), resulting in k_H/k_D values of 3.26 and 2.78, respectively. The kinetic isotope effect indicated that the C–H cleavage was indeed a hydrogen atom transfer process and might occur at the rate-determining step of the reaction.[51]

Table 1 Photocatalytic α-amino C–H arylation with different catalysts under standard conditions[a]

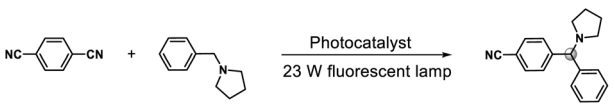

Entry	Photocatalysts	Conversion (%)
1	Cd-**MIX**	98 (93[b])
2	None	No reaction
3	$Cd(NO_3)_2\cdot 4H_2O$	No reaction
4	H_3**TCA** + **NPy$_3$**	27
5	H_3**TCA** + **NPy$_3$** + $Cd(NO_3)_2\cdot 4H_2O$	32
6	Cd-**TCA**	16
7	Cd-**NPy$_3$**	49
8	Cd-**TCA** + **NPy$_3$**	19
9	Cd-**NPy$_3$** + H_3**TCA**	48
10	Cd-**TCA** + Cd-**NPy$_3$**	53

[a] Catalyst (0.5 mol%, based on the Ar_3N moiety, Cd salt is based on the molar ratio to Ar_3N in Cd-**MIX**), 1,4-DCB (1.0 mmol), NaOAc (1.0 mmol), amine **1c** (2.0 mmol), and 4.0 mL of DMSO for 10 h. Conversions were determined by GC-MS. [b] Isolated yield.

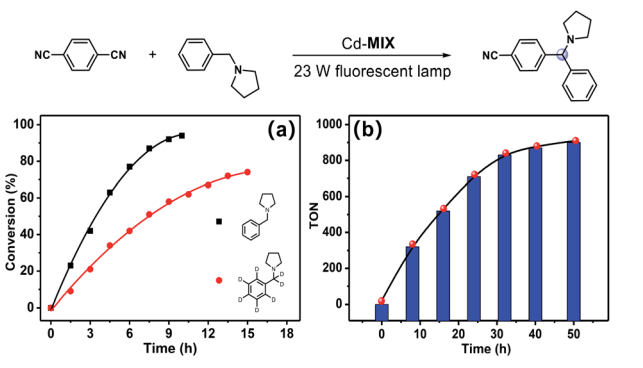

Fig. 4 (a) Kinetics curves of the C–H arylation using *N*-benzylpyrrolidine or *N*-((phenyl-D_5)methyl-D_2)pyrrolidine with 1,4-dicyanobenzene under optimal conditions. (b) The turnover number in scale-up experiments for C–H arylation of *N*-benzylpyrrolidine with 1,4-dicyanobenzene (0.64 g) within 50 h under optimal conditions.

Compared to typical direct HAT photocatalysis in which the activated photocatalyst acts as a HAT catalyst to abstract a H atom from a substrate,[12] our approach, in which the *in situ* formed oxidized $Ar_3N^{\bullet+}$ acts as a HAT catalyst, possibly avoids the use of a strong oxidizer to abstract the H-atom from the substrate and diminishes the direct oxidization of the substrate to form a byproduct. It is noted that the H-atom abstraction agents in previously reported SET/HAT synergistic photocatalysis have always been transient radical species generated either through electron transfer or energy transfer by photocatalysts.[52] Our approach thus simplified the transformation steps by using the oxidized state of the photosensitizer itself for the H-atom abstraction, representing a new HAT strategy parallel to direct HAT catalysis in which the excited state of the photocatalyst behaves as a HAT catalyst for H-atom abstraction.[53]

Besides the advantages of fewer constituents and decreased reaction steps, the new heterogeneous photoredox-mediated HAT approach exhibits recyclability of the heterogeneous photocatalyst.[54] We adopted a model fluidized bed reactor[55] for C–H arylation of amine compounds to investigate the recycling properties of Cd-**MIX**: after one round of reaction, the reaction solution was removed, and then fresh reaction solution containing substrates was added for another round of reaction. No significant decrease in conversion was observed after three cycles (Fig. S36 and S37†). The similar powder X-ray diffraction patterns of the synthesized and recovered Cd-**MIX** confirmed that the polymer structure was maintained (Fig. S40†). By adding excess substrates, 5.0 mmol of 1,4-dicyanobenzene and 10.0 mmol of *N*-benzylpyrrolidine (**1c**), the loading of 0.1 mol% Cd-**MIX** (based on the Ar_3N moiety) gave a TON value of about 900 per mole of catalyst after 50 hours of irradiation. The total pseudo-first order kinetics behavior (rate constant $k = 0.048 \pm 0.004$ h^{-1}) demonstrated that the catalytic efficiency was maintained after 50 hours of constant irradiation (Fig. 4b and S39†). There was no obvious variation in catalytic efficiency when the size of Cd-**MIX** was reduced from 200 to 1.0 μm by mechanical grinding. We infer that the surface area of the catalyst is not a crucial factor for the arylation reaction (Fig. S41†). Therefore, Cd-**MIX** is a real heterogeneous photocatalyst that allows the catalytic reaction to occur in the channels of the coordination polymer.

As functional benzylic amines are important building blocks in pharmaceuticals,[56] scope exploration began with a change in amines (Table 2). Piperidines and morpholines provided desirable results (88% and 83%). Acyclic amines were converted with moderate conversions (74% and 68%). Meanwhile, amines with benzyl groups resulted in good conversions to *N*-benzylic arylation products with high regioselectivity. Several electron-deficient arenes or heteroaromatic benzonitriles as coupling substrates could also undergo coupling with amines (**1a** and **1c**), forming the corresponding products when 1.0 mol% Cd-**MIX** was used. The results indicated that Cd-**MIX** as a new heterogeneous photoredox HAT catalyst can achieve efficient conversion *via* photocatalysis and excellent regioselectivity *via* HAT catalysis, which has not been reported for regioselective functionalization of C(sp^3)–H bonds.

Table 2 Photocatalytic α-amino C–H arylation with selected amines and benzonitriles

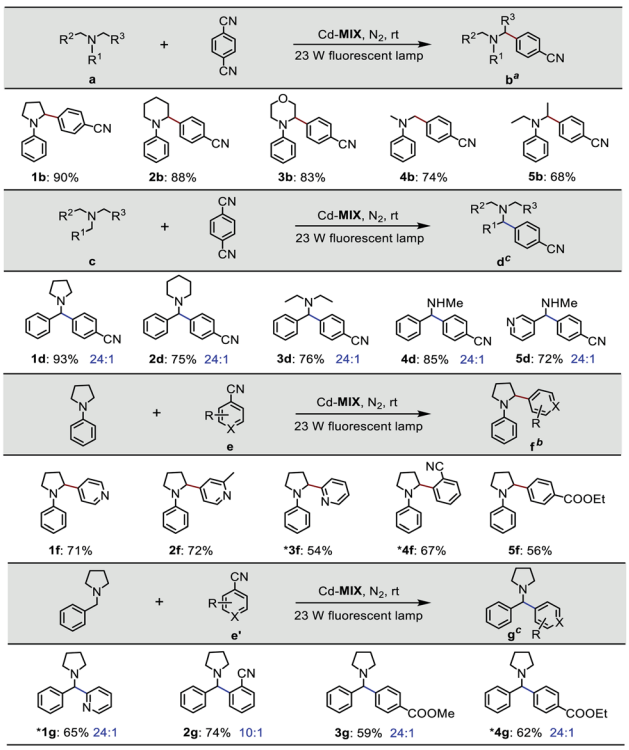

[a] Reaction conditions: catalyst (0.5 mol%, based on the Ar_3N moiety), 1,4-DCB (1.0 mmol), NaOAc (1.0 mmol), amine (2.0 mmol), and 4.0 mL of DMAC for 12 h. [b] Catalyst (1.0 mol%, based on the Ar_3N moiety), arenes (0.5 mmol), NaOAc (0.5 mmol), amine (1.0 mmol), and 2.0 mL of DMAC for 12 h. [c] DMSO for 10 h. *0.2 mmol scale. Conversions were determined by ^1H NMR. The regioselectivity was determined by GC-MS.

To further explore the potential factors affecting the new direct HAT strategy, monoligand coordination polymers Cd-**TCA** and Cd-**NPy_3** were used as reference photocatalysts (Fig. 5). Cd-**NPy_3** has a 2D layered structure, while Cd-**TCA** is a 3D framework consolidated by pentanuclear Cd-clusters with

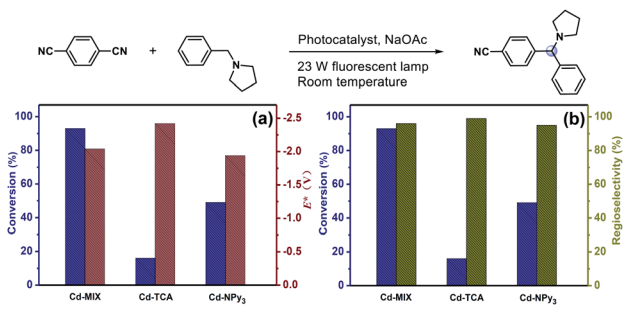

Fig. 5 (a) Conversions of the C–H arylation of **1c** using Cd-**MIX**, Cd-**TCA**, and Cd-**NPy_3** as catalysts and the excited state potentials of the three coordination polymers under optimal conditions. (b) Conversions of the C–H arylation of **1c** using Cd-**MIX**, Cd-**TCA**, and Cd-**NPy_3** as catalysts and the regioselectivity of *N*-benzyl arylation products under optimal conditions.

channel openings of 7.7 × 8.1 Å^2 (Fig. S6†). PXRD analyses indicated that the bulk samples of Cd-**TCA** and Cd-**NPy$_3$** consisted of a pure phase (Fig. S18†). Dye adsorption experiments on the two monoligand coordination polymers revealed that the layered Cd-**NPy$_3$** has a poor adsorption effect, while the porous Cd-**TCA** has comparable adsorption ability to Cd-**MIX** (Fig. S22†). Control experiments demonstrated that conversions of 20% and 35% with **1a** as the substrate, or 16% and 49% with **1c** as the substrate were obtained using Cd-**TCA** and Cd-**NPy$_3$** as catalysts, respectively (Tables S4 and S5,† entries 6 and 7). The higher catalytic efficiency of Cd-**NPy$_3$** than that of Cd-**TCA** demonstrated that the different porous behaviors of the coordination polymers were not the important factors dominating the catalytic behavior directly.

When one monoligand polymer was mixed with another free ligand as a photocatalyst, such as Cd-**TCA** with **NPy$_3$** or Cd-**NPy$_3$** with H$_3$**TCA**, the conversions of the reaction were not ideal under the same conditions (Tables S4 and S5,† entries 8 and 9). The photocatalytic efficiency of the mixture of Cd-**TCA** and Cd-**NPy$_3$** was still lower than that of the mixed-ligand Cd-**MIX** (Tables S4 and S5,† entries 10). Solid-state cyclic voltammetry of Cd-**TCA** (0.53 V) and Cd-**NPy$_3$** (0.75 V) (*vs.* Ag/AgCl) (Fig. S20 and S21†) revealed that the oxidation potentials of both were less positive than those of **1a** and **1c** (Fig. 3b), and the excited state potentials of Cd-**TCA** (−2.42 V) and Cd-**NPy$_3$** (−1.94 V) were both sufficient to reduce 1,4-dicyanobenzene (Fig. 5a). We concluded that it is not the redox potential but the special structural intermediate that mixed both N(sp^3) and N(sp^2) characteristics of the central nitrogen atom, which decreased the structural relaxation from $Ar_3N^{\bullet+}$ to Ar_3NH^+ in the mixed-ligand coordination polymer Cd-**MIX**, dominates the differentiation of catalytic performance of the aforementioned coordination polymers, which is consistent well with the idea of a mechanistic switchover from SET to HAT catalysis. The proton-coupled electron transfer mechanism,[57,58] in which a proton and an electron are exchanged in a concerted elementary step, which would require a deprotonation step of **1a** and **1c** ahead of the oxidation event, was precluded.

Considering the difference in spectral properties of Cd-**MIX**, Cd-**TCA**, and Cd-**NPy$_3$** (Fig. 3a), a comparison of the photocatalytic efficiency of the three catalysts was conducted under LED irradiation with three single wavelengths (365 nm, 395 nm, and 420 nm). As expected, when irradiated by a 365 nm LED with **1a** or **1c** as the substrate, all three catalysts were able to achieve complete transformation of 1,4-dicyanobenzene (Tables S4 and S5,† entries 15), but byproducts were present owing to excessive activation by the strong irradiation (Fig. S42 and S43†). When irradiated by a 395 nm (or 420 nm) LED with **1a** or **1c** as the substrate, Cd-**MIX** gave high conversions (>95%) based on 1,4-dicyanobenzene, but the catalytic conversions by Cd-**TCA** and Cd-**NPy$_3$** were both lower than those of Cd-**MIX** (Tables S4 and S5,† entries 16 and 17). When using a household fluorescent lamp that closely matches natural light as the light source, the gap in the catalytic efficiency of the three photocatalysts gradually widened (Tables S4 and S5,† entries 1, 6, and 7). We infer that the mixed-ligand approach was of great significance to extend the absorption spectra of the catalysts, in addition to the favourable photosensitivity and the HAT performance, which is beneficial for the synergistic SET/HAT catalysis to proceed under visible light irradiation.

Transient photocurrent/time tests revealed that Cd-**MIX** produces a higher photocurrent response than Cd-**TCA** and Cd-**NPy$_3$** (Fig. 6a), indicating that Cd-**MIX** has a higher electron–hole (e–h) separation efficiency. As photoinduced excitons are active only after effective charge separation,[59] the higher photocurrent response of Cd-**MIX** indicates the higher photocatalytic activity.[60] Electrochemical impedance spectroscopy plots showed that Cd-**MIX** has lower transport resistance than Cd-**TCA** and Cd-**NPy$_3$** (Fig. 6b). The faster electron transfer rate in the mixed-ligand polymer Cd-**MIX** would be another factor endowing higher catalytic efficiency.[21,61] We concluded that the mixed-ligand approach first improved the photochemical and photophysical properties over two monoligand polymers, and then improved the photocatalytic efficiency of the C–H arylation reaction, which provided insights into the rational design and optimization of recyclable photocatalysts for rapid access to complex bioactive molecules and late-stage functionalized pharmaceuticals.

^{1}H NMR of the desolvated Cd-**MIX** immersed in a methanol solution of **1a** and **1c** revealed that Cd-**MIX** could adsorb these substrates within its pores (in DMSO-d$_6$/DCl, Fig. S30a and 31a†). The IR spectra of Cd-**MIX** adsorbed with **1a** and **1c** showed characteristic signals at 2973–2869 cm^{-1} and 2961–2732 cm^{-1}, demonstrating the adsorption and activation of the substrates within the pores of Cd-**MIX** (Fig. S30b and 31b†). The crystal structures of the regular crystals of **1a**- and **1c**-impregnated Cd-**MIX** (denoted as **1a**@Cd-**MIX** and **1c**@Cd-**MIX**) provided activation information for elucidating the mechanism details.[28,62]

As shown in Table S1,† the uptake of substrates **1a** or **1c** did not influence the main structure of the framework, and the cell dimensions and pores were retained. In **1a**@Cd-**MIX**, the amines were located close to the **NPy$_3$** moiety; they were

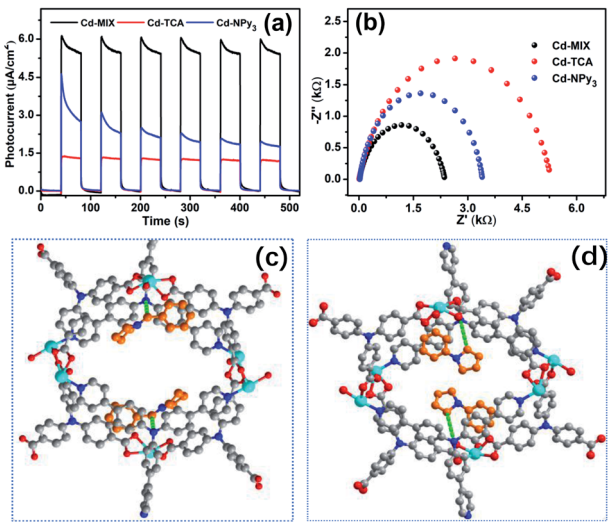

Fig. 6 Photocurrent tests (a) and EIS plots (b) of Cd-**MIX**, Cd-**TCA**, and Cd-**NPy$_3$** under the same conditions, showing the superiority of Cd-**MIX** over the others. The interaction patterns between the embedded substrates (**1c** and **1a**) and active sites in the channels of **1c**@Cd-**MIX** (c) and **1a**@Cd-**MIX** (d).

inserted between the layers of molecular sheets and interacted with the phenyl rings of **NPy$_3$** *via* π···π stacking interactions with an interplanar separation of approximately 3.75 Å (Fig. 6d and S12†). The α-position of **1a** was positioned near the central N atom of **NPy$_3$**, reflecting that the well-positioned **NPy$_3$** ligands in Cd-**MIX** should be the active sites for the HAT event. When the trapped substrates contained an *N*-benzyl group (**1c**), the embedded amine molecules were adjusted into a suitable conformation to allow the phenyl rings of **NPy$_3$** and **1c** to stack with an interplanar separation of 3.66 Å (Fig. 6c and S13†). In addition, there is also a weak interaction between the phenyl rings of **1c** and the **TCA**$^{3-}$ ligand, and the vertical π···π stacking distance is approximately 3.72 Å (Fig. S13†). Such double π···π stacking interactions provided a driving force for the amine to approach the active sites. Substrate **1c** can be docked near the central N atom of **NPy$_3$** by the C–H···N interactions between *N*-alkyl and central N as well as between *N*-benzyl and central N (*ca.* 3.87 Å and 3.40 Å), which facilitates the *in situ* formed oxidized **NPy$_3$**$^{\bullet+}$ to abstract a H atom from the benzyl C–H bond of **1c**. These results support our hypothesis that the strong interaction between the amines and photocatalyst is an important factor in promoting catalytic conversion. The interactions between the amines and active sites in the channels of the polymer accelerate the capture of the substrate amines and lock the amines around the catalytic sites,[24] facilitating the generation of amine radicals through the activation of *N*-alkyl and *N*-benzyl C–H bonds by the HAT process.

Conclusions

In summary, we have reported a mixed-ligand approach to the construction of dual functional coordination polymers which enables the arylation of α-amino C(sp^3)–H bonds in a predictable, regioselective and recyclable manner. The different molecular sizes and coordination modes of the two Ar_3N-containing ligands consolidate and optimize the Ar_3N moieties into special structural intermediates, facilitating the oxidized $Ar_3N^{\bullet+}$ to abstract a hydrogen atom from C(sp^3)–H nucleophiles, which is not capable of proceeding on a homogeneous triarylamine-based photocatalyst. The new direct SET/HAT strategy endows the electron transfers *via* a synergistic effect and skips several interactions between transient species during the typical synergistic SET/HAT cycles, demonstrating a promising redox-economical and reagent-economical heterogeneous photocatalytic platform that has not been reported for α-amino C–H arylation to form benzylamine derivatives. The mixed-ligand approach improves the photochemical and photophysical properties over two monoligand coordination polymers, providing deep insights into the rational design and optimization of recyclable photocatalysts for rapid access to complex bioactive molecules and late-stage functionalized pharmaceuticals.

Experimental section

Materials and measurements

Unless stated otherwise, all chemicals and solvents were of reagent grade quality obtained from commercial sources and used without further purification. H_3**TCA** and **NPy$_3$** were synthesized using previously reported procedures.[27,63] Cd-**TCA** was synthesized according to a published procedure.[42]

Elemental analyses of C, N, and H were performed on a Vario EL III elemental analyzer. Powder X-ray diffraction (PXRD) tests were performed on a SmartLab 9kW X-ray diffractometer instrument with a Cu sealed tube. Fourier transform infrared spectroscopy (IR) spectra were recorded using KBr pellets on a JASCO FT/IR-430 instrument. ^{1}H NMR and ^{13}C NMR spectra were recorded on a Varian INOVA 400 M spectrometer. Solution and solid-state UV-vis spectra were obtained on TU-1900 and Hitachi U-4100 spectrophotometers. Thermogravimetric analyses (TGA) were carried out at a ramp rate of 10 °C min^{-1} up to 800 °C under a nitrogen flow with a Mettler-Toledo TGA/SDTA851 instrument.

Scanning electron microscopy (SEM) images were taken using a HITACHI UHR FE-SEM SU8200 microscope. Fluorescence spectra were collected on an EDINBURGH F900 instrument. GC analyses were performed on an Agilent Technologies 6890 N GC system. Electron paramagnetic resonance (EPR) experiments were performed on a Bruker E500 instrument, and the intensity was recorded at 100 K under an Ar atmosphere. Cyclic voltammograms (CV) and electrochemical impedance spectroscopy (EIS) plots were measured on a ZAHNER ENNIUM electrochemical workstation. Transient photocurrent/time measurements were performed on a CHI 650E electrochemical workstation. Confocal laser scanning microscopy micrographs were collected using an Olympus Fluoview FV1000 instrument.

Preparation of coordination polymers

Synthesis of Cd-MIX. A mixture of H_3**TCA** (19.0 mg, 0.05 mmol), **NPy$_3$** (24.0 mg, 0.05 mmol), and $Cd(NO_3)_2\cdot 4H_2O$ (77.0 mg, 0.25 mmol) was dissolved in a mixed solvent of DMF, acetonitrile, and H_2O in an autoclave. The resulting mixture was kept in an oven at 110 °C for 72 h. After cooling the autoclave to room temperature, bright yellow lamellar crystals were obtained. Yield: 50%. Prolonging the reaction time or changing the molar ratio between the two ligands will not affect the formation of the structure, but will affect the purity and yield of the crystals. Anal. calcd for $C_{78}H_{57}Cd_3N_7O_{15}$: C, 56.11; H, 3.44; N, 5.87%. Found: C, 56.10; H, 3.54; N, 5.81%. IR/cm^{-1} (KBr): 3062 (w), 3037 (w), 1594 (s), 1523 (br, m), 1390 (s), 1315 (m), 1174 (m), 813 (w), 782 (m).

Syntheses of 1a@Cd-MIX and 1c@Cd-MIX. Cd-**MIX** was first soaked in a methanol solution (48 h) to remove guest molecules and then fully dried in a vacuum oven (100 °C, 1 h). **1a**@Cd-**MIX** and **1c**@Cd-**MIX** were obtained by soaking the activated Cd-**MIX** in a methanol solution containing **1a** and **1c** (10.0 mmol) for 48 h, respectively.

Synthesis of Cd-NPy$_3$. A mixture of **NPy$_3$** (12.0 mg, 0.025 mmol) and $CdCl_2\cdot 2.5H_2O$ (29.0 mg, 0.13 mmol) was dissolved in a mixed solvent of DMF, acetonitrile, and H_2O in an autoclave. The resulting mixture was kept in an oven at 100 °C for 72 h. After cooling the autoclave to room temperature, pale yellow block-shaped crystals of Cd-**NPy$_3$** were obtained. Yield: 56%.

Single crystal X-ray crystallography

Data of Cd-**MIX**, **1a**@Cd-**MIX**, **1c**@Cd-**MIX**, and Cd-$\mathbf{NPy_3}$ were measured on a Bruker SMART APEX CCD diffractometer with Mo-Kα radiation (λ = 0.71073 Å) using the SMART and SAINT programs.[64,65] The crystal structures were solved by direct methods and then refined by full-matrix least-squares refinements on F^2 using SHELXL-97 software. And an absorption correction was performed using the SADABS program.[66] The remaining atoms were found from successive full-matrix least-squares refinements on F^2 and Fourier syntheses. Non-H atoms were refined with anisotropic displacement parameters. H atoms in the backbones were fixed geometrically at calculated distances and allowed to ride on the parent non-hydrogen atoms, whereas some of the disordered solvent molecules were not treated during the structural refinements. To help the stability of the refinement for the impregnated related substrate molecules, the bond distances between several atoms were fixed, and thermal parameters on adjacent atoms in two molecules were restrained to be similar. The SQUEEZE program was carried out for Cd-**MIX**, **1a**@Cd-**MIX**, and **1c**@Cd-**MIX**. The crystallographic data for Cd-**MIX**, **1a**@Cd-**MIX**, **1c**@Cd-**MIX**, and Cd-$\mathbf{NPy_3}$ are summarized in Table S1.†

Catalysis details

Before catalysis experiments, solvent exchange experiments of catalysts were carried out to activate the catalysts. First, fresh catalysts were immersed in a methanol solution for 48 h and then fully dried out in a vacuum oven (373 K) for 10 h to obtain the activated catalysts.

General procedure for the photocatalytic C–H arylation

Arylation of amines with 1,4-dicyanobenzene. A glass tube was filled with 1,4-dicyanobenzene (1.0 mmol), photocatalyst (0.5 mol%, based on the Ar_3N moiety), NaOAc (1.0 mmol), amine (2.0 mmol), and solvent (4.0 mL). Then the reaction mixture was cooled to −78 °C, degassed and backfilled with N_2 three times. The resulting mixture was stirred and irradiated with a 23 W fluorescent lamp at room temperature. The conversions were determined by ^{1}H NMR analyses, and the regioselectivity was determined by GC-MS. The conversions of the optimization process of experimental conditions were determined by GC-MS.

Arylation of amines with heteroaromatic benzonitriles and electron-deficient arenes. A glass tube was filled with heteroaromatic benzonitriles and electron-deficient arenes (0.5 mmol), photocatalyst (1.0 mol%, based on the Ar_3N moiety), NaOAc (0.5 mmol), amine (1.0 mmol), and solvent (2.0 mL). Then the reaction mixture was cooled to −78 °C, degassed and backfilled with N_2 three times. The resulting mixture was stirred and irradiated with a 23 W fluorescent lamp at room temperature. The conversions were determined by ^{1}H NMR analyses, and the regioselectivity was determined by GC-MS.

Deuterium labeling experiments. The deuterium labeling experiments were carried out by using *N*-((phenyl-D_5)methyl-D_2) pyrrolidine (**1c***D*) instead of **1c** as the coupling partner with 1,4-dicyanobenzene under optimal conditions. The conversions were determined by ^{1}H NMR analyses.

General procedure for the consecutive photocatalytic C–H arylation. A glass tube was filled with 1,4-dicyanobenzene (5.0 mmol), photocatalyst (0.1 mol%, based on the Ar_3N moiety), NaOAc (5.0 mmol), amine (10.0 mmol), and solvent (20.0 mL). Then the reaction mixture was cooled to −78 °C, degassed and backfilled with N_2 three times. The resulting mixture was stirred and irradiated with a 23 W fluorescent lamp at room temperature for 50 or 60 h.

Author contributions

C. Duan conceived the project, designed the experiments and supervised the work. H. Li and X. Jing carried out the main experiments, collected and interpreted the data. Y. Yang and C. He solved and refined the X-ray single crystal structures. All authors discussed the results and commented on the manuscript.

Conflicts of interest

There are no conflicts to declare.

Acknowledgements

This work was supported by the National Natural Science Foundation of China (21890381 and 21971030).

Notes and references

1 Y. Qin, L. H. Zhu and S. Z. Luo, *Chem. Rev.*, 2017, **117**, 9433–9520.
2 M. A. Ashley, C. Yamauchi, J. C. K. Chu, S. Otsuka, H. Yorimitsu and T. Rovis, *Angew. Chem., Int. Ed.*, 2019, **58**, 4002–4006.
3 L. Marzo, S. K. Pagire, O. Reiser and B. König, *Angew. Chem., Int. Ed.*, 2018, **57**, 10034–10072.
4 D. M. Schultz and T. P. Yoon, *Science*, 2014, **343**, 1239176.
5 A. Hossiain, A. Bhattacharyya and O. Reiser, *Science*, 2019, **364**, eaav9713.
6 D. Ravelli, D. Dondi, M. Fagnoni and A. Albini, *Chem. Soc. Rev.*, 2009, **38**, 1999–2011.
7 J. M. R. Narayanam and C. R. J. Stephenson, *Chem. Soc. Rev.*, 2011, **40**, 102–113.
8 C. Le, Y. F. Liang, R. W. Evans, X. M. Li and D. W. C. MacMillan, *Nature*, 2017, **547**, 79–83.
9 A. H. Hu, J. J. Guo, H. Pan and Z. W. Zuo, *Science*, 2018, **361**, 668–672.
10 L. Capaldo and D. Ravelli, *Eur. J. Org. Chem.*, 2017, 2056–2071.
11 J. M. Mayer, *Acc. Chem. Res.*, 2011, **44**, 36–46.
12 X. Z. Fan, J. W. Rong, H. L. Wu, Q. Zhou, H. P. Deng, J. D. Tan, C. W. Xue, L. Z. Wu, H. R. Tao and J. Wu, *Angew. Chem., Int. Ed.*, 2018, **57**, 8514–8518.
13 J. J. Murphy, D. Bastida, S. Paria, M. Fagnoni and P. Melchiorre, *Nature*, 2016, **532**, 218–222.
14 Y. Y. Shen, Y. T. Gu and R. Martin, *J. Am. Chem. Soc.*, 2018, **140**, 12200–12209.

15 C. Gao, J. Wang, H. X. Xu and Y. J. Xiong, *Chem. Soc. Rev.*, 2017, **46**, 2799–2823.
16 C. Yang, R. Li, K. A. I. Zhang, W. Lin, K. Landfester and X. C. Wang, *Nat. Commun.*, 2020, **11**, 1239.
17 L. Capaldo, L. L. Quadri and D. Ravelli, *Green Chem.*, 2020, **22**, 3376–3396.
18 X. Yu and S. M. Cohen, *J. Am. Chem. Soc.*, 2016, **138**, 12320–12323.
19 X. J. Yang, T. Liang, J. X. Sun, M. J. Zaworotko, Y. Chen, P. Cheng and Z. J. Zhang, *ACS Catal.*, 2019, **9**, 7486–7493.
20 C. Y. Xu, Y. T. Pan, G. Wan, H. Liu, L. Wang, H. Zhou, S. H. Yu and H. L. Jiang, *J. Am. Chem. Soc.*, 2019, **141**, 19110–19117.
21 T. Zhang and W. B. Lin, *Chem. Soc. Rev.*, 2014, **43**, 5982–5993.
22 A. Dhakshinamoorthy, Z. H. Li and H. Garcia, *Chem. Soc. Rev.*, 2018, **47**, 8134–8172.
23 L. Zeng, T. Liu, C. He, D. Y. Shi, F. L. Zhang and C. Y. Duan, *J. Am. Chem. Soc.*, 2016, **138**, 3958–3961.
24 Z. Q. Xia, C. He, X. G. Wang and C. Y. Duan, *Nat. Commun.*, 2017, **8**, 361.
25 B. Z. Lü, Y. F. Chen, P. Y. Li, B. Wang, K. Müllen and M. Z. Yin, *Nat. Commun.*, 2019, **10**, 767.
26 (*a*) Y. X. Tan, Y. P. He, D. Q. Yuan and J. Zhang, *Appl. Catal., B*, 2018, **221**, 664–669; (*b*) X. K. Wang, J. Liu, L. Zhang, L. Z. Dong, S. L. Li, Y. H. Kan, D. S. Li and Y. Q. Lan, *ACS Catal.*, 2019, **9**, 1726–1732.
27 P. Y. Wu, C. He, J. Wang, X. J. Peng, X. Z. Li, Y. L. An and C. Y. Duan, *J. Am. Chem. Soc.*, 2012, **134**, 14991–14999.
28 T. X. Zhang, X. Y. Guo, Y. S. Shi, C. He and C. Y. Duan, *Nat. Commun.*, 2018, **9**, 4024.
29 X. H. Zhang and D. W. C. MacMillan, *J. Am. Chem. Soc.*, 2017, **139**, 11353–11356.
30 B. Adelizzi, I. A. W. Filot, A. R. A. Palmans and E. W. Meijer, *Chem.–Eur. J.*, 2017, **23**, 6103–6110.
31 J. L. Jeffrey, J. A. Terrett and D. W. C. MacMillan, *Science*, 2015, **349**, 1532–1536.
32 J. Twilton, M. Christensen, D. A. DiRocco, R. T. Ruck, I. W. Davies and D. W. C. MacMillan, *Angew. Chem., Int. Ed.*, 2018, **57**, 5369–5373.
33 H. K. Chae, J. Kim, O. D. Friedrichs, M. O'Keeffe and O. M. Yaghi, *Angew. Chem., Int. Ed.*, 2003, **42**, 3907–3909.
34 Z. Q. Yao, J. Xu, B. Zou, Z. P. Hu, K. Wang, Y. J. Yuan, Y. P. Chen, R. Feng, J. B. Xiong, J. L. Hao and X. H. Bu, *Angew. Chem., Int. Ed.*, 2019, **58**, 5614–5618.
35 H. Seo, M. H. Katcher and T. F. Jamison, *Nat. Chem.*, 2017, **9**, 453–456.
36 L. Shi and W. J. Xia, *Chem. Soc. Rev.*, 2012, **41**, 7687–7697.
37 Y. Mori, Y. Sakaguchi and H. Hayashi, *J. Phys. Chem. A*, 2000, **104**, 4896–4905.
38 Y. C. Qiu, S. Yuan, X. X. Li, D. Y. Du, C. Wang, J. S. Qin, H. F. Drake, Y. Q. Lan, L. Jiang and H. C. Zhou, *J. Am. Chem. Soc.*, 2019, **141**, 13841–13848.
39 H. Jiang, J. t Jia, A. Shkurenko, Z. J. Chen, K. Adil, Y. Belmabkhout, L. J. Weselinski, A. H. Assen, D. Xu Xue, M. O'Keeffe and M. Eddaoudi, *J. Am. Chem. Soc.*, 2018, **140**, 8858–8867.
40 A. L. Spek, *J. Appl. Crystallogr.*, 2003, **36**, 7–13.
41 T. L. Easun, F. Moreau, Y. Yan, S. H. Yang and M. Schröder, *Chem. Soc. Rev.*, 2017, **46**, 239–274.
42 Y. Shen, X. F. Yang, H. B. Zhu, Y. Zhao and W. S. Li, *Dalton Trans.*, 2015, **44**, 14741–14746.
43 (*a*) M. A. Nasalevich, M. G. Goesten, T. J. Savenije, F. Kapteijna and J. Gascon, *Chem. Commun.*, 2013, **49**, 10575–10577; (*b*) Y. Lee, S. Kim, J. K. Kang and S. M. Cohen, *Chem. Commun.*, 2015, **51**, 5735–5738.
44 T. Ide, J. P. Barham, M. Fujita, Y. Kawato, H. Egami and Y. Hamashima, *Chem. Sci.*, 2018, **9**, 8453–8460.
45 G. J. Kavarnos, *Fundamentals of Photoinduced Electron Transfer*, VCH, New York, 1993.
46 D. Rehm and A. Weller, *Isr. J. Chem.*, 1970, **8**, 259–271.
47 J. R. Lakowicz, *Principles of Fluorescence Spectroscopy*, 1999.
48 (*a*) A. McNally, C. K. Prier and D. W. C. MacMillan, *Science*, 2011, **334**, 1114–1117; (*b*) M. T. Pirnot, D. A. Rankic, D. B. C. Martin and D. W. C. MacMillan, *Science*, 2013, **339**, 1593–1596.
49 W. Z. Liu and F. G. Bordwell, *J. Org. Chem.*, 1996, **61**, 4778–4783.
50 Y. R. Luo, *Comprehensive Handbook of Chemical Bond Energies*, CRC Press, Boca Raton, 2007.
51 E. M. Simmons and J. F. Hartwig, *Angew. Chem., Int. Ed.*, 2012, **51**, 3066–3072.
52 A. Dewanji, P. E. Krach and M. Rueping, *Angew. Chem., Int. Ed.*, 2019, **58**, 3566–3570.
53 D. M. Yan, J. R. Chen and W. J. Xiao, *Angew. Chem., Int. Ed.*, 2019, **58**, 378–380.
54 A. Bavykina, N. Kolobov, I. S. Khan, J. A. Bau, A. Ramirez and J. Gascon, *Chem. Rev.*, 2020, **120**, 8468–8535.
55 M. M. Bello, A. A. Abdul Raman and M. Purushothaman, *J. Cleaner Prod.*, 2017, **141**, 1492–1514.
56 A. Trowbridge, S. M. Walton and M. J. Gaunt, *Chem. Rev.*, 2020, **120**, 2613–2692.
57 J. M. Mayer, *Annu. Rev. Phys. Chem.*, 2004, **55**, 363–390.
58 T. Hoshikawa and M. Inoue, *Chem. Sci.*, 2013, **4**, 3118–3123.
59 H. Liu, C. Y. Xu, D. D. Li and H. L. Jiang, *Angew. Chem., Int. Ed.*, 2018, **57**, 5379–5383.
60 D. Y. Shi, R. Zheng, M. J. Sun, X. R. Cao, C. X. Sun, C. J. Cui, C. S. Liu, J. W. Zhao and M. Du, *Angew. Chem., Int. Ed.*, 2017, **56**, 14637–14641.
61 T. Song, L. Zhang, P. Y. Zhang, J. Zeng, T. T. Wang, A. Alia and H. P. Zeng, *J. Mater. Chem. A*, 2017, **5**, 6013–6018.
62 T. Kawamichi, T. Haneda, M. Kawano and M. Fujita, *Nature*, 2009, **461**, 633–635.
63 C. Hua, A. Baldansuren, F. Tuna, D. Collison and D. M. D'Alessandro, *Inorg. Chem.*, 2016, **55**, 7270–7280.
64 SMART, *Data collection software (version 5.629)*, Bruker AXS Inc., Madison, WI, 2003.
65 SAINT, *Data reduction software (version 6.54)*, Bruker AXS Inc., Madison, WI, 2003.
66 G. M. Sheldrick, *SHELXTL97, Program for crystal structure solution*, University of Göttingen, Göttingen, Germany, 1997.